Journal of proteome research

pubs.acs.org/jpr

Article

Quantitative Proteomic Analysis of Porcine Intestinal Epithelial Cells Infected with Porcine Deltacoronavirus Using iTRAQ-Coupled LC-MS/MS

Xinrong Zhou, Lei Zhou, Xinna Ge, Xin Guo, Jun Han, Yongning Zhang,* and Hanchun Yang*

Cite This: *J. Proteome Res.* 2020, 19, 4470–4485

Read Online

ACCESS | Metrics & More | Article Recommendations | Supporting Information

ABSTRACT: Porcine deltacoronavirus (PDCoV) is an emergent enteropathogenic coronavirus associated with swine diarrhea. Porcine small intestinal epithelial cells (IPEC) are the primary target cells of PDCoV infection in vivo. Here, isobaric tags for relative and absolute quantification (iTRAQ) labeling coupled to liquid chromatography–tandem mass spectrometry (LC-MS/MS) was used to quantitatively identify differentially expressed proteins (DEPs) in PDCoV-infected IPEC-J2 cells. A total of 78 DEPs, including 23 upregulated and 55 downregulated proteins, were identified at 24 h postinfection. The data are available via ProteomeXchange with identifier PXD019975. To ensure reliability of the proteomics data, two randomly selected DEPs, the downregulated anaphase-promoting complex subunit 7 (ANAPC7) and upregulated interferon-induced protein with tetratricopeptide repeats 1 (IFIT1), were verified by real-time PCR and Western blot, and the results of which indicate that the proteomics data were reliable and valid. Bioinformatics analyses, including GO, COG, KEGG, and STRING, further demonstrated that a majority of the DEPs are involved in numerous crucial biological processes and signaling pathways, such as immune system, digestive system, signal transduction, RIG-I-like receptor, mTOR, PI3K-AKT, autophagy, and cell cycle signaling pathways. Altogether, this is the first study on proteomes of PDCoV-infected host cells, which shall provide valuable clues for further investigation of PDCoV pathogenesis.

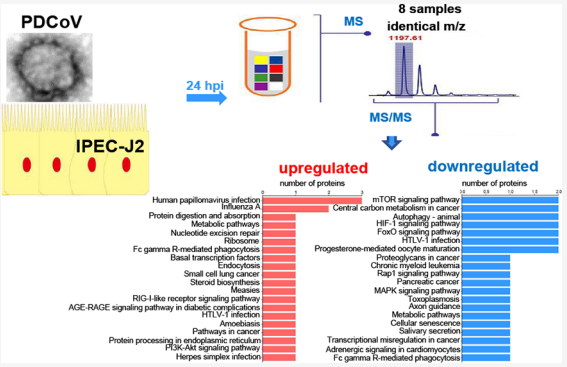

KEYWORDS: *porcine deltacoronavirus (PDCoV), IPEC-J2 cells, isobaric tags for relative and absolute quantification (iTRAQ), liquid chromatography–tandem mass spectrometry (LC-MS/MS), proteome*

1. INTRODUCTION

Porcine deltacoronavirus (PDCoV) is enveloped and has a single-stranded, positive-sense RNA genome, which is classified in the genus *Deltacoronavirus* within the *Coronaviridae* family.[1] Although PDCoV was initially identified in rectal swabs of pigs during a molecular epidemiological investigation conducted in Hong Kong, China in 2012,[2] diarrheal diseases in pigs associated with PDCoV infection were first recorded in the U.S. in 2014.[3] Since then, the virus has been detected in many other countries, including Canada, mainland China, South Korea, Thailand, Laos, Vietnam, Japan, Mexico, and so on.[4,5] Clinically, PDCoV-infected pigs often present with diarrhea and/or vomiting, dehydration, and death of neonatal piglets.[6] The outbreak of PDCoV infection in numerous countries has resulted in considerable economic losses to the global swine industry.[7]

PDCoV has an obvious enteropathogenic characteristic in pigs.[1,6] The small intestine of pigs, in particular the jejunum and ileum, are the primary target organs of PDCoV, and porcine small intestinal epithelial cells (IPEC) are the main sites of PDCoV replication in vivo.[1,8,9] Histopathologic analyses showed that PDCoV infection not only causes villus atrophy and fall-off but also leads to necrosis of small intestinal enterocytes in infected pigs.[1,6] Currently, an immortalized, nontumorigenic IPEC-J2 cell line, originally established using the jejunum of a newborn unsuckled piglet,[10] has been shown to exhibit high similarities to porcine intestinal primary epithelial cells,[11] and thus can better simulate the porcine physiological state than any other cell lines. At present, IPEC-J2 cells have been successfully utilized as an ideal in vitro model system for investigating the interactions between epithelial cells and porcine enteric viruses, such as porcine rotavirus,[12] porcine endemic diarrhea virus (PEDV),[13] and transmissible gastroenteritis virus (TGEV).[14] Recently, Jung and colleagues demonstrated that IPEC-J2 cells are quite susceptible to PDCoV infection in vitro.[8]

Special Issue: Proteomics in Pandemic Disease

Received: August 2, 2020
Published: October 12, 2020

As a newly emerged swine enteropathogenic coronavirus, the pathogenic mechanisms of PDCoV are still poorly documented and warrant further exploration.[1] It is well-known that when a virus invades a host cell, complex interactions between the host cell and the virus will occur. On the one hand, the invading virus subverts some of the cellular biological functions in favor of the replication of the virus itself; on the other, the cells adopt various defense strategies to fight against the invading virus.[15] The whole process of virus−cell interactions is usually accompanied by changes of genomics, transcriptomics, and proteomics.[16] Recently, a systematic transcriptome analysis of PDCoV-infected PK-15 cells was conducted using high-throughput RNA sequencing, and 3762 differentially expressed genes were identified, most of which participate in the innate immunity and the corresponding signal transduction pathways.[17] As of yet, however, no proteomic data are currently available for PDCoV-infected cells.

Proteomics is an effective tool for the comprehensive analysis of host cellular responses to viral infections, which is conducive to elucidating the underlying pathogenesis of the virus.[18] The currently available proteomics techniques include two-dimensional gel electrophoresis,[15] two-dimensional difference gel electrophoresis,[19] stable isotope labeling by amino acids in cell culture,[20,21] isobaric tags for relative and absolute quantitation (iTRAQ),[22] and label-free proteomic techniques.[23] Among all these mentioned techniques, iTRAQ coupled with liquid chromatography−tandem mass spectrometry (LC-MS/MS) analysis has shown several comparative advantages over its counterparts, for instance, high sensitivity, high throughput, high separating capacity, and high accuracy, and thus emerged as a robust quantitative proteomics technique for the comprehensive analysis of differentially expressed proteins (DEPs). To date, this technique has been successfully applied to numerous studies involved in virus-host interactions, examples of which include TGEV,[22] PEDV,[24] foot-and-mouth disease virus (FMDV),[25] porcine circovirus type 2 (PCV2), and classical swine fever virus (CSFV).[26] These studies have given a good overview of the dynamic interactions between the virus and its host, and provide important clues for a better understanding of the viral pathogenesis. For PDCoV, there has been no proteomic study on the virus so far. In the present study, we coupled iTRAQ with LC-MS/MS to quantitatively analyze the DEPs of IPEC-J2 cells in response to PDCoV infection. The identified DEPs were subsequently analyzed by comprehensive bioinformatics analyses.

2. MATERIALS AND METHODS

2.1. Virus, Cells, and Antibodies

The PDCoV CHN-HN-1601 strain (GenBank access no. MG832584) used in this study was isolated from the intestinal contents of a piglet with diarrhea using porcine kidney LLC-PK1 cells in 2017. The eighth passage of PDCoV with a titer of $10^{8.45}$ 50% tissue culture infectious dose ($TCID_{50}$)/mL was used for virus inoculation. IPEC-J2 cells were generously provided by Prof. Yongchang Cao (School of Life Sciences, Sun Yat-Sen University, Guangzhou, China). The cells were cultivated in Dulbecco's Modified Eagle Medium/Ham's F-12 (DMEM/F12) (Gibco, Carlsbad, CA, USA) containing 10% fetal bovine serum (FBS; Gibco, Carlsbad, CA, USA), 5 μg/mL insulin, 5 μg/mL transferrin, 5 ng/mL selenium (Sigma-Aldrich, St. Louis, MO, USA), 100 U/mL penicillin and 0.1 mg/mL streptomycin (Solarbio Life Sciences, Beijing, China). Cells were cultured at 37 °C in a humidified CO_2 incubator (Thermo Fisher Scientific, Waltham, MA, USA). The monoclonal antibody (mAb), 1A3, raised against the PDCoV nucleocapsid protein was prepared in our laboratory. Mouse anti-β-actin mAb, mouse anti-IFIT1 and rabbit anti-ANAPC7 polyclonal antibodies were bought from Abcam (Cambridge, MA, USA). Horseradish peroxidase (HRP)-conjugated goat antimouse/rabbit immunoglobulin G (IgG) were obtained from Sigma-Aldrich. Alexa Fluor 488-conjugated goat anti-mouse IgG was the product of Thermo Fisher Scientific.

2.2. Virus Inoculation

IPEC-J2 cells approaching ∼80% confluence were washed twice with sterile phosphate buffered saline (PBS; 0.01 M, pH 7.4), and then mock infected or infected with PDCoV CHN-HN-1601 strain at a multiplicity of infection (MOI) of 0.1 $TCID_{50}$ per cell. After adsorption for 1.5 h at 37 °C, the cells were rinsed once with sterile PBS and serum-free DMEM/F12 medium containing 5 μg/mL of trypsin (Sigma-Aldrich) was added. The cells were further cultured at 37 °C for the specified time points until different assays had been performed. Viral propagation in IPEC-J2 cells was evaluated by observing cytopathic effect (CPE), determination of one-step growth curve and immunofluorescence assay (IFA) using the mAb 1A3 against PDCoV.

2.3. $TCID_{50}$ Assay

The kinetics of PDCoV multiplication in IPEC-J2 cells was determined by measuring the $TCID_{50}$ using a microtitration infectivity assay. Briefly, 100 μL/well of 10-fold serial dilutions of PDCoV were inoculated onto IPEC-J2 cells grown in 96-well microplates (Corning, NY, USA). After adsorption at 37 °C for 1.5 h, the inocula were removed, and serum-free DMEM/F12 medium containing 5 μg/mL of trypsin was added to the wells. After an additional 48-h cultivation, virus titers were measured by observing the presence of visible CPEs in the corresponding wells, and calculated using the Reed−Muench method.[27]

2.4. IFA

When IPEC-J2 cells grown in 96-well microplates reached ∼80% confluence, they were mock infected or infected with PDCoV at an MOI of 0.1 $TCID_{50}$ per cell. After a 48-h cultivation at 37 °C with 5% CO_2, the cells were fixed with prechilled 100% ethanol for 15 min at room temperature. After washing with PBS, the cells were probed with the mAb 1A3 (1:5000 dilution) at 37 °C for 1 h. Following another washing step, 1000-fold-diluted Alexa Fluor 488-conjugated goat antimouse IgG (Thermo Fisher Scientific) was added to the cells and incubated at 37 °C for 1 h. After washing thrice with PBS, cells were observed with an Eclipse Ci-S microscope (Nikon Corp., Tokyo, Japan).

2.5. Protein Extraction, Digestion, and iTRAQ Labeling

At 24 h postinfection (hpi), both PDCoV- and mock-infected IPEC-J2 cells grown in T25 flasks (∼5×10^6 cells/flask) were rinsed twice with prechilled PBS, and then harvested with disposable cell scrapers. Three flasks of each group (PDCoV or mock) were harvested and used as three independent biological replicates. After centrifugation at 300*g* for 10 min, the cell pellets from each flask were lysed with 800 μL of RIPA lysis buffer (Beyotime, Shanghai, China) containing 1% SDS, 8 M urea and protease inhibitors (Beyotime). The cell lysates

https://dx.doi.org/10.1021/acs.jproteome.0c00592
J. Proteome Res. 2020, 19, 4470−4485

were further sonicated on ice for 5 min with 10 s bursts and 10 s pauses between cycles. After centrifugation for 20 min at 12 000*g* and 4 °C, the supernatant was collected and used as the total cellular proteins. The concentration of protein samples was determined using a Pierce BCA protein assay kit (Thermo Scientific, Rockford, IL, USA).

The total cellular proteins from each biological replicate were equally divided into three aliquots, which were used as three independent technical replicates for the LC-MS/MS runs. For tryptic digestion and iTRAQ labeling, an aliquot of each protein sample containing ∼100 μg of total cellular proteins was adjusted to a 100-μL final volume using the RIPA lysis buffer. A final concentration of 10 mM of tris (2-carboxyethyl) phosphine (TCEP) was added to each protein sample, which was then incubated at 37 °C for 1 h. Afterward, iodoacetamide was added at a final concentration of 40 mM, and the protein solution was incubated for 40 min at room temperature shielded from light. Subsequently, prechilled acetone was added to the protein solution in a ratio of 6:1 and precipitated at −20 °C for 4 h. After centrifugation (10 000*g*, 4 °C) for 20 min, the precipitate was dissolved with 100 μL of 100 mM triethylammonium bicarbonate (TEAB). The processed protein samples were digested with 2 μg/μL of trypsin overnight at 37 °C. Following tryptic digestion, the generated peptides were dried by vacuum centrifugation, and redissolved with 20 μL of 0.5 M TEAB. The prepared peptides were then labeled with an iTRAQ reagents-8 plex kit (AB Sciex, Foster City, CA, USA) as per the manufacturer's protocol. Briefly, the three independent biological replicates of mock-infected cellular samples were each labeled with iTRAQ-113, iTRAQ-114, and iTRAQ-115; the three independent biological replicates of PDCoV-infected samples were each labeled with iTRAQ-116, iTRAQ-119, and iTRAQ-121. All the labeled samples of each group were mixed with an equal amount, and then fractionated using an ACQUITY ultra performance liquid chromatography (UPLC) system (Waters Corp., Milford, MA, USA) combined with an ACQUITY UPLC BEH C18 column (300 Å, 1.7 μm, 2.1 mm × 150 mm). Finally, a total of 10 fractions of each group were collected. After merging two fractions of each group into one, the pooled 10 fractions were dried by using a rotary vacuum concentrator.

2.6. LC-MS/MS Analysis

LC-MS/MS analyses of the labeled peptides were carried out using a Q-Exactive mass spectrometer (Thermo Fisher Scientific, San Jose, CA, USA) combined with an EASY-nLC 1200 system (Thermo Fisher Scientific). After loading 2 μg of the labeled peptides onto a C18 reversed phase HPLC column (Thermo Fisher Scientific), peptides were chromatographed for 120 min at a flow rate of 300 nL/min over gradients from 2−80% (mobile phase A comprising 0.1% (v/v) formic acid and 2% (v/v) acetonitrile; mobile phase B comprising 0.1% (v/v) formic acid and 80% (v/v) acetonitrile). The following ion source parameters, including spray voltage 1.8 kV, capillary temperature 275 °C and declustering potential 100 V, were set. The mass spectrometer was run using a data-dependent Top-20 acquisition mode, switching automatically between MS and MS/MS. A full MS scan ranging from 350 to 1300 m/z was conducted at 70 000 resolution with an automatic gain control (AGC) target value of 3×10^6 ions and a maximum ion transfer (IT) of 20 ms. The precursor ions were fragmented by means of high-energy collisional dissociation (HCD), and all MS/MS spectra were scanned using the following parameters: resolution 17 500; AGC 1×10^5 ions; maximum IT 50 ms; dynamic exclusion duration 18 s; normalized collision energy 30%; and intensity threshold 1.6×10^5.

2.7. MS Data Analysis

The original MS/MS raw data were analyzed using the Proteome Discoverer Software 2.1 (Thermo Fisher Scientific, San Jose, CA, USA). The data were searched against the database of UniProt *Sus scrofa* (February 26, 2017, containing 26 103 sequences, http://www.uniprot.org/proteomes/UP000008227, version: Uniprot-proteome-UP000008227-Sus scrofa (Pig)-26103s-20170226.fasta) and porcine deltacoronavirus Uniprot database (February 26, 2017, containing 442 sequences, http://www.uniprot.org/porcinedeltacoronavirus, version: Uniprot-Porcine deltacoronavirus [1586324]-442s-20170226.fasta). The parameters for database searching were set as follows: instrument, TripleTOF 5600; cysteine alkylation, iodoacetamide; digestion, trypsin; dynamic modification, oxidation (M), acetylation (protein N-terminus), and iTRAQ8plex (Y); static modification, iTRAQ8plex (K), iTRAQ8plex (N-terminus), and carbamidomethyl (C); maximum missed cleavages, 2; precursor mass tolerance, 10 ppm; fragment mass tolerance, 0.05 Da; validation based on, *q*-value. To guarantee the accuracy of the MS data analysis, the cutoff value for the peptide and protein confidences was set to >95% and >1.20, respectively, coupled with a false discovery rate (FDR) of ≤1% for peptide and protein identifications. The *t* test function in the *R* language software was applied to calculate the *p*-value of the expression difference of cellular proteins between mock- and PDCoV-infected IPEC-J2 cells, and only proteins with a fold change >1.20 or <0.83 and a *p*-value < 0.05, which have being widely used as the criteria for judging DEPs,[28,29] were considered differentially expressed.

2.8. Bioinformatics Analysis

The data for the identified DEPs of PDCoV-infected IPEC-J2 cells were submitted to Gene Ontology (GO) Terms (http://geneontology.org/) for GO analysis, by which the DEPs were assigned into three branches of ontology—biological process (BP), cellular component (CC), and molecular function (MF). GO enrichment analysis for the DEPs was done using the Goatools software (https://github.com/tanghaibao/GOatools) with Fisher's exact test, and those with a *p*-value < 0.05 were thought to be significantly enriched. The protein database of clusters of Orthologous Groups (COG; http://www.ncbi.nlm.nih.gov/COG/) was also used to assign possible functions to the identified DEPs. The Kyoto Encyclopedia of Genes and Genomes (KEGG; http://www.genome.jp/kegg/) pathway analyses were performed to reveal the potential functions of the DEPs, which were annotated using the BlastP program of the Diamond software against the KEGG database with a cutoff *E*-value ≤ 1×10^{-5} and identity ≥0.98. The pathway enrichment statistics were performed using the KOBAS software (http://kobas.cbi.pku.edu.cn/home.do/) with the Fisher's exact test, and those with *p*-values < 0.05 were regarded as statistically significant.[30,31] Furthermore, the protein−protein interaction networks were created using the online STRING database (http://string-db.org/) and visualized by Cytoscape (https://cytoscape.org/), which was widely used for analyzing the relationships between DEPs.[32]

2.9. Quantitative Real-Time PCR (qPCR)

To verify the DEPs identified by iTRAQ at the transcriptional level, the mRNA of two representative DEPs, the down-

https://dx.doi.org/10.1021/acs.jproteome.0c00592
J. Proteome Res. 2020, 19, 4470−4485

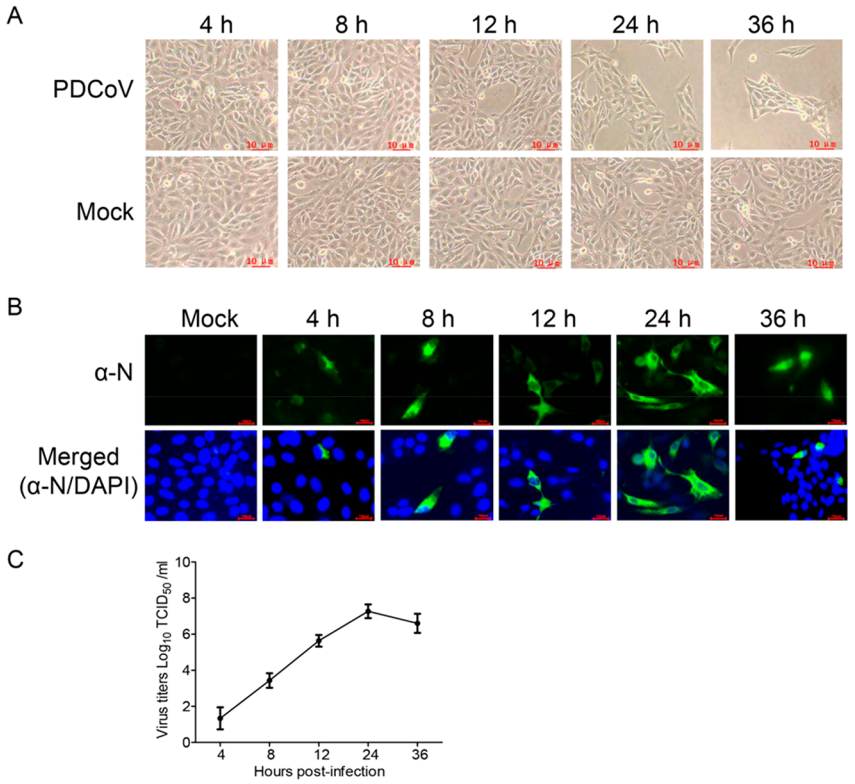

Figure 1. Proliferation of PDCoV in IPEC-J2 cells. (A) Morphological changes in IPEC-J2 cells infected with the PDCoV CHN-HN-1601 strain at an MOI of 0.1 $TCID_{50}$/cell or mocked infected for 4, 8, 12, 24, and 36 h, respectively. Scale bars, 10 μm. (B) Confirmation of PDCoV proliferation in IPEC-J2 cells by immunofluorescence assays using the mAb 1A3 specific for PDCoV (α-N) and an Alexa Fluor 488-labeled goat antimouse IgG, and mock-infected cells at 24 h was used as a negative control. Cell nuclei were counterstained with DAPI (blue). Scale bars, 10 μm. (C) One-step growth curve of PDCoV in IPEC-J2 cells at the indicated time points following viral infection. The titer of virus was presented as $TCID_{50}$/mL, and the data were recorded as means ± SD from three independent experiments.

regulated ANAPC7 and the upregulated IFIT1, were detected by qPCR. Total cellular RNA of both PDCoV- and mock-infected IPEC-J2 cells was extracted using the TaKaRa MiniBEST universal RNA extraction kit (Dalian, China). The first strand cDNA was synthesized using 2 μg of cellular RNA and with a RevertAid First Strand cDNA Synthesis Kit (Thermo Scientific) following the manufacturer's instructions. The qPCR assays were conducted using a TaKaRa SYBR Premix Ex Taq kit on an ABI 7500 real-time PCR machine along with β-actin as a housekeeping gene. The primers used for the qPCR assay were designed based on the NCBI reference sequences for ANAPC7, IFIT1 and β-actin genes under GenBank accession numbers NM_016238, HQ679904 and NM_001101, respectively. The information for the designed primers was as following: ANAPC7 (Forward: 5′-CTTTGCTGAGGAACGCACTG-3′, Reverse: 5′-TCCATGTCGTCCACATCCTC-3′); IFIT1 (Forward: 5′-GAAGATTTAACCCAACAAGAACATA-3′, Reverse: 5′-CTTTCGATACGTAAGGTAATACAGC-3′); β-actin (Forward: 5′-TCCCTGGAGAAGAGCTACGA-3′, Reverse: 5′-AGCACTGTGTTGGCGTACAG-3′). The qPCR assays were carried out in a 20-μL reaction volume comprised 10 μL of TaKaRa SYBR Premix Ex Taq, 0.4 μL of each forward and reverse primer (10 μM), 7.2 μL of nuclease-free water, and 2 μL of template. The qPCR amplifications were carried out using a thermal profile with an initial step at 95 °C for 2 min, followed by 40 cycles of 95 °C for 10 s, 60 °C for 10 s (for ANAPC7 and β-actin) or 55 °C for 10 s (for IFIT1) and 72 °C for 40 s. Fold-change values were calculated in term of the $2^{-\Delta\Delta Ct}$ method and normalized to the β-actin reference gene.[33]

2.10. Western Blot Analysis

To further validate the identified DEPs, Western blot was performed to detect ANAPC7 and IFIT1 protein expression levels using β-actin as an internal control. Briefly, total cellular proteins were extracted from both mock- and PDCoV-infected IPEC-J2 cells at 24 hpi. The resulting protein samples were separated on 12% SDS-PAGE gels and transferred onto 0.22 μm poly(vinylidene fluoride) (PVDF) membranes (Millipore, Bedford, MA, USA) using a semidry electrophoretic transfer cell (Bio-Rad, Hercules, CA, USA). The membranes were blocked with 5% (w/v) nonfat dry milk overnight at 4 °C and then probed with either anti-ANAPC7 (1:1000), anti-IFIT1 (1:1000), or anti-β-actin (1:5000) primary antibodies at 37 °C for 1 h. After thorough washing with PBST, the membranes were incubated with the corresponding HRP-conjugated secondary antibodies (1:8000) for 1 h at 37 °C. The target protein blots on the membranes were developed with an enhanced chemiluminescence detection kit (Thermo Fisher Scientific), and images were taken using a ProteinSimple FluorChem E image system (Santa Clara, CA, USA).

2.11. Data Availability

The proteomics data obtained by LC-MS/MS in this study were deposited to the ProteomeXchange Consortium (http://proteomecentral.proteomexchange.org) by means of the Proteomics Identifications (PRIDE) partner repository with the data set identifier PXD019975.

https://dx.doi.org/10.1021/acs.jproteome.0c00592
J. Proteome Res. 2020, 19, 4470−4485

Table 1. Differentially Expressed Proteins Identified by iTRAQ Analysis of IPEC-J2 Cells in Response to PDCoV Infection

protein name	Uniprot accession no.	$\log_2$ ratios (infection/control)	peptides	sequence coverage (%)	*p*-values	functions
Upregulated proteins in PDCoV-infected cells						
ISG15 ubiqutin-like modifier	I3LU39	1.24	18	30.1	3.62×10^{-06}	RIG-1/MDA5 mediated induction of IFN-alpha/beta pathways
Interferon-stimulated protein 60	F1SCY2	1.09	5	14.6	3.51×10^{-05}	Defense response to virus
2′-5′ oligoadenylates synthetase 1, OAS1	F1RJN6	0.81	2	3.1	0.0001	Antiviral protein
Radical *S*-adenosyl methionine domain-containing protein 2	F1S9L2	0.70	6	13.8	1.60×10^{-05}	Defense response to virus
Interferon induced protein with tetratricopeptide repeats 1, IFIT1	K7GN56	0.70	5	9.6	0.0002	Regulation of defense response to virus
Family with sequence similarity 8 member A1	F1RUH9	0.69	1	2.2	0.0103	unknown
uncharacterized protein	I3LH89	0.658	1	4.7	0.0074	unknown
Interferon-induced GTP-binding protein Mx1	K7GKN2	0.58	2	2.0	0.0013	GTPase activity; cellular response to type I interferon
Nucleoporin 37 (NUP37)	F1SRJ4	0.57	1	5.2	0.0016	Transporting macromolecules
Nuclear transcription factor Y submit beta (NFYB)	F1SG36	0.55	2	6.3	0.0013	DNA-binding transcription factor activity
DNA excision repair protein ERCC-6-like isoform a (ERCC6L)	I3LFY4	0.45	1	0.8	0.0496	DNA translocase activity
Collagen type IV alpha 1 chain	F1RLM1	0.45	1	0.6	0.0153	Component of glomerular basement membranes (GBM)
Ribouclease T2	F1SBX8	0.35	2	4.4	0.0004	Ribinuclease T2 activity
MRPL32	I3LTC4	0.34	1	11.7	0.0472	translation
Phostensin	Q767M0	0.32	3	6.8	0.0047	Phosphatase binding
Bridging integrator 1	F1RXZ6	0.32	7	22.7	0.0012	Regulation of endocytosis
Terpene cyclase/mutase family member	I3L7C2	0.29	10	16.7	0.0012	Beta-amyrin synthase activity
Secretagogin (SCGN)	Q06A97	0.28	2	9.4	0.0214	Calcium binding
Interleukin 13 receptor subunit alpha 2	K7GSC6	0.28	2	14.6	0.0370	Obsolete signal transducer activity and cytokine receptor activity
FOS-like 1 (FOSL1)	F1RU26	0.28	1	6.2	0.0214	DNA-binding transcription factor activity
Prolactin regulatory element binding	F1SED4	0.27	9	10.1	0.0229	GTPase activator activity
CDK-activating kinase assembly factor MAT1 (MNAT1)	F6Q8T7	0.27	1	6.4	0.0076	DNA-dependent ATPase activity
Intraflagellar transport 81	F1RNN4	0.26	1	3.7	0.0033	Tubulin binding
Downregulated proteins in PDCoV-infected cells						
Very low density lipoprotein receptor (VLDLR)	E7CXS1	−0.27	21	22.8	0.0001	Apolipoprotein binding
uncharacterized	I3LFU8	−0.27	3	5.6	0.0218	unknown
Myeloid leukemia factor 2	F1SLT1	−0.28	6	15.8	0.0488	DNA-binding
Helicase-like transcription factor (HLTF)	I3LM88	−0.28	1	1.9	0.0254	DNA-dependent ATPase activity
Ras association domain family member 6	F1RUL8	−0.29	2	5.5	0.0011	Regulation of apoptotic process
Nucleoside diphosphate kinase 7 (NME7)	F1RPV8	−0.29	3	8.0	0.0279	Synthesis of nucleoside triphosphates
Bromodomain adjacent to zinc finger domain 2A (BAZ2A)	F1SLA2	−0.29	1	1.2	0.0189	Component of the nucleolar remodeling complex
BMP2 inducible kinase	I3LT15	−0.29	1	2.8	0.0319	Protein kinase activity
RNA helicase (DDX55)	F1RFL5	−0.29	1	1.5	0.0274	Catalytic activity
TMEM55B	F1S8H7	−0.29	1	3.9	0.0445	Catalytic activity
Chromatin assembly factor 1 subunit A (CHAF1A)	F1S7L7	−0.29	4	5.3	0.0252	Chromo shadow domain binding
RNA polymerase II subunit A C-terminal domain phosphatase (CTDP1)	F1RWS7	−0.29	2	5.5	0.0123	Promoting the activity of RNA polymerase II
uncharacterized	I3LIB8	−0.30	2	14.7	0.0373	unknown
Intraflagellar transport 172	I3LPC6	−0.30	1	0.69	0.0383	Negative regulation of epithelial cell proliferation
Myocyte enhancer factor 2D (MEF2D)	F1RP31	−0.30	1	1.9	0.0418	Protein dimerization activity
Poly(ADP-ribose) glycohydrolase	F1SDW4	−0.31	1	1.3	0.0355	Poly(ADP-ribose) glycohydrolase activity
Mitogen-activated protein kinase 4	F1STG5	−0.31	4	4.9	0.0233	Protein serine/threonine kinase activity

https://dx.doi.org/10.1021/acs.jproteome.0c00592
J. Proteome Res. 2020, 19, 4470−4485

Table 1. continued

protein name	Uniprot accession no.	log_2 ratios (infection/control)	peptides	sequence coverage (%)	*p*-values	functions
Anaphase promoting complex subunit 7 (ANAPC7)	I3L7Q8	−0.31	4	7.9	0.0218	Ubiquitin protein ligase activity
Transmembrane protein 45A	F1SKZ6	−0.31	1	3.6	0.0191	Modulates cancer cell chemosensitivity
Katanin p60 ATPase-containing subunit A1	I3LVP8	−0.32	2	32.1	0.0181	ATPase activity
Ubiquitin associated protein 2 (UBAP2)	F1SEA5	−0.32	1	1.7	0.0237	Cadherin binding
Ribosomal RNA adenine dimethylase domain containing 1	F1RHJ0	−0.32	1	2.3	0.0391	rRNA (adenine-N6,N6)-dimethyltransferase activity
Lemur tyrosine kinase 2	F1RFL2	−0.32	1	1.0	0.0104	Protein serine/threonine kinase activity
Poly(ADP-ribose) polymerase family member 10	F1RSK9	−0.32	1	1.8	0.0182	K63-linked polyubiquitin modification-dependent protein binding
CDK9	C9E1C9	−0.32	4	11.0	0.0183	Cyclin-dependent protein serine/threonine kinase activity
Cystatin C	Q0Z8R0	−0.33	2	17.1	0.0282	Cysteine-type endopeptidase inhibitor activity
Cyclin and CBS domain divalent metal cation transport mediator 2	F1S849	−0.33	1	1.1	0.0173	Adenylnucleotide binding
Protein-serine/threonine kinase	F1S069	−0.34	4	8.2	0.0247	Protein serine/threonine kinase activity
Aamy domain-containing protein	F1S5K2	−0.34	1	2.5	0.0390	Catalytic activity; amino acid transport
GATOR complex protein WDR24	I3LF05	−0.34	1	1.4	0.0368	Regulation of autophagy; positive regulation of TOR signaling
CD109 antigen isoform 1 preproprotein	K7GKY0	−0.35	18	12.9	0.0105	Endopeptidase inhibitor activity
Nonspecific serine/threonine protein kinase (AKT2)	G9BWQ2	−0.35	7	12.0	0.0310	Transferase activity
DNA polymerase delta interacting protein 3 (POLDIP3)	F1SJQ4	−0.35	3	3.8	0.0287	RNA binding
Exostosin-like glycosyltransferase 2	F1S568	−0.35	1	3.3	0.0215	Transferase activity
4F5 domain-containing protein	I3LS25	−0.36	9	42.4	0.0015	Positive regulator of amyloid protein aggregation and proteotoxicity
Integrator complex subunit 4 (INTS4)	F1STY6	−0.37	3	2.4	0.0429	Involved in the small nuclear RNAs (snRNA) U1 and U2 transcription
Smoothelin-like 2	F1RGN8	−0.37	1	2.7	0.0119	Actin cytoskeleton organization
Elongation of very long chain fatty acids protein	I3L7S8	−0.39	1	21.6	0.0444	Catalytic activity
uncharacterized	I3LBD1	−0.40	1	7.4	0.0085	unknown
Secretory carrier-associated membrane protein	F1SJ46	−0.41	7	13.1	0.0144	Protein transport
Cadherin 6	F1SP42	−0.42	3	3.7	0.0122	Calcium ion binding
Superoxide dismutase	I3LUD1	−0.43	2	4.9	0.0139	Superoxide dismutase activity
Probable ribosome biogenesis protein C16orf42 homologue (SMARCA2)	F1RFZ6	−0.44	1	4.4	0.0470	Involved in ribosome biogenesis
Protein zyg-11 homologue B	F1S6I1	−0.45	1	3.4	0.0030	Positive regulation of proteasomal ubiquitin-dependent protein catabolic process
BCL2 interacting protein 3	I3LDJ9	−0.45	2	6.6	0.0009	Protein homodimerization activity
Alpha-(1,6)-fucosyltransferase (FUT8)	F1SA54	−0.47	1	3.3	0.0492	Alpha-(1→6)-fucosyltransferase activity
Signal peptide peptidase-like 2B	F1S8G9	−0.52	2	1.9	0.0190	Protein homodimerization activity
INTS3 and NABP interacting protein (INTS4)	F1SNA6	−0.54	5	12.5	0.0006	DNA repair
Trypsin domain containing 1	F1SUE6	−0.55	1	1.8	0.0215	Serine-type endopeptidase activity
UDP-glucose glycoprotein glucosyltransferase 2	F1RP50	−0.62	2	2.3	0.0320	Glycoprotein glucosyltransferase activity
Phosphatidylglycerophosphate synthase 1	I3LN95	−0.62	1	2.7	0.0440	Calcium ion binding
Metallothionein-2A	P79379	−0.63	9	32.8	0.0017	Metal ion binding
uncharacterized	I3LNY1	−0.66	1	6.5	0.0246	unknown
Formin-like 1	I3LH80	−0.83	1	1.8	0.0191	Rho GTPase binding
uncharacterized	K7GL96	−1.13	1	10.9	0.0412	unknown

2.12. Statistical Analysis

The methods used for the statistical analysis of proteomic data and the corresponding threshold criteria were described in detail in the corresponding sections of MS data and bioinformatics analyses. The data from three independent qPCR runs were expressed as means ± standard deviation (SD), and were statistically analyzed by Student's *t* test using the GraphPad Prism software (Version 5.0; La Jolla, CA,

https://dx.doi.org/10.1021/acs.jproteome.0c00592
J. Proteome Res. 2020, 19, 4470−4485

USA). Differences with a value of $p < 0.05$ were regarded as statistically different.

3. RESULTS

3.1. Determination of the Optimal Inoculation Dose for PDCoV

To obtain the optimal inoculation dose that could produce DEPs to the greatest extent, IPEC-J2 cells were inoculated with PDCoV at low, medium, and high MOIs (i.e., 0.01, 0.1, and 1 $TCID_{50}$/cell, respectively) for 36 h before the formal experiment. By observing the CPE, we found that the high MOI resulted in a rapid synchronous infection of all the cells, causing majority of the cells detached and disintegrated within 12 hpi. This is not conducive to the interaction between the virus and the cells. By contrast, the cells inoculated with the low MOI only displayed minimal CPEs at the same time points, which might induce limited changes in the expression levels of diverse proteins. Therefore, the medium MOI of 0.1 was selected as the optimal dose for PDCoV inoculation in all subsequent experiments.

3.2. Selection of the Best Sampling Time for the Proteomic Analysis Following PDCoV Infection

In order to determine the optimal time point for the proteomic analysis following PDCoV infection, IPEC-J2 cells were inoculated with PDCoV at an MOI of 0.1 and microscopically observed for CPE at 4, 8, 12, 24, and 36 hpi. Meanwhile, the cell supernatants at the same time points were collected and used to measure the proliferation dynamics of PDCoV in IPEC-J2 cells. Compared to mock-infected cells, PDCoV-inoculated IPEC-J2 cells began to exhibit slight CPE at 8 hpi, and the CPE gradually became increasingly evident as the infection progressed. Obvious CPEs were observed at 12 hpi and became more evident at 24 and 36 hpi, which were characterized by cell rounding, enlarging, and granular degeneration of the cytoplasm that occurred either singly or in different-sized clusters, usually forming cell masses, followed by cell shrinkage and increased detachment. These CPEs were in agreement with those reported by Jung et al.,[8] and resembled those observed in PDCoV-infected swine testicular (ST) and LLC-PK1 cells.[34] However, from 36 hpi onward, the majority of the cells became detached and floated in the medium (Figure 1A). The proliferation of PDCoV in IPEC-J2 cells was verified by IFA using a mAb raised against the PDCoV nucleocapsid protein, and the results demonstrated that almost all cells became infected at 24 hpi (Figure 1B). The one-step growth curve further revealed that the virus titer reached a plateau of $\sim 10^{7.5}$ $TCID_{50}$/mL at 24 hpi, followed by a gradual and continuous decline (Figure 1C). In general, the time point at which viral proliferation stays high but no obvious cellular membrane or cytoskeleton rearrangement occurs is the optimal sampling time for a proteomic analysis.[22] On the basis of the above experimental results, we therefore chose 24 hpi as the optimal time point for the proteomic analysis of PDCoV-infected IPEC-J2 cells.

3.3. Identification of DEPs of IPEC-J2 Cells in Response to PDCoV Infection

To identify the DEPs following viral infection, the total cellular proteins extracted from PDCoV- and mock-infected IPEC-J2 cells were processed for quantitative proteomics research using iTRAQ-coupled LC-MS/MS technique. In all, 5502 cellular proteins were identified in both PDCoV- and mock-infected IPEC-J2 cells at 24 hpi (Supplementary File S1). On the basis of the widely used criteria for judging DEPs (fold changes >1.2 or <0.83 and with $p < 0.05$),[28,29] 23 proteins were significantly upregulated and 55 proteins were markedly downregulated in PDCoV-infected IPEC-J2 cells in comparison with the mock-infected cells (Table 1). Meanwhile, six viral proteins, including the nucleocapsid protein, spike protein, membrane protein, 3C-like proteinase Nsp5, accessory proteins NS6 and NS7 (Supplementary File S2), were also identified in PDCoV-infected IPEC-J2 cells by searching against the porcine deltacoronavirus Uniprot database. In order to ensure the reliability of the obtained proteomic data, three biological replicates of PDCoV- or mock-infected cell samples were collected and three technical replicates were performed during the proteomic analysis. The difference was plotted against the percentage of the identified proteins, which suggested that the proteomic data had high credibility (Supplementary Figure S1). Notably, due to the fact that the current genome database of pigs is inadequately annotated in comparison to the human genome database, we found six uncharacterized or unassigned proteins among the 78 DEPs (Table 1). Therefore, a functional analysis of these proteins warrants further investigation.

3.4. Validation of the DEPs by qPCR and Western Blot Analyses

To validate the obtained LC-MS/MS data, qPCR was performed to evaluate the transcription levels of two randomly selected DEPs, the downregulated ANAPC7 and the upregulated IFIT1. To this end, IPEC-J2 cells were mock-infected or infected with PDCoV at an MOI of 0.1. At 24 hpi, total cellular RNA was extracted from the cells and subjected to qPCR assays. As shown in Figure 2A, the level of mRNA encoding ANAPC7 and IFIT1 proteins was significantly downregulated and upregulated in PDCoV-infected cells, respectively, as compared to the mock-infected cells ($p < 0.05$). The qPCR results were in agreement with the MS data which were acquired by the iTRAQ approach (Figure 2B). For further confirmation of the proteomic data, the expression level of ANAPC7 and IFIT1 proteins in IPEC-J2 cells, which were infected exactly as the aforementioned conditions, was also tested by Western blot analysis. To track the progression of PDCoV infection, the mAb 1A3 that specifically recognizes PDCoV was utilized. As shown in Figure 2C, compared with the mock-infected IPEC-J2 cells, PDCoV significantly decreased the expression of ANAPC7 protein and its relative ratio to β-actin in the cells, whereas the expression of IFIT1 protein and its relative ratio to β-actin in the cells were significantly increased as a consequence of PDCoV infection. The original images of the entire PVDF membranes containing the target Western blots were included in Supplementary Figure S2. The Western blot results were also consistent with the MS data (Figure 2D). Taken together, these experimental results reveal that our quantitative proteomics data are quite reliable.

3.5. GO Functional Annotation of the DEPs

To characterize the DEPs, GO analysis was conducted to annotate the proteins based on three major categories: biological process (BP), cellular component (CC), and molecular function (MF). Within the BP category, the proteins were predicted to be involved in 13 biological processes, including immune system process, reproductive process, biological adhesion, multiorganism process, detoxification,

https://dx.doi.org/10.1021/acs.jproteome.0c00592
J. Proteome Res. 2020, 19, 4470−4485

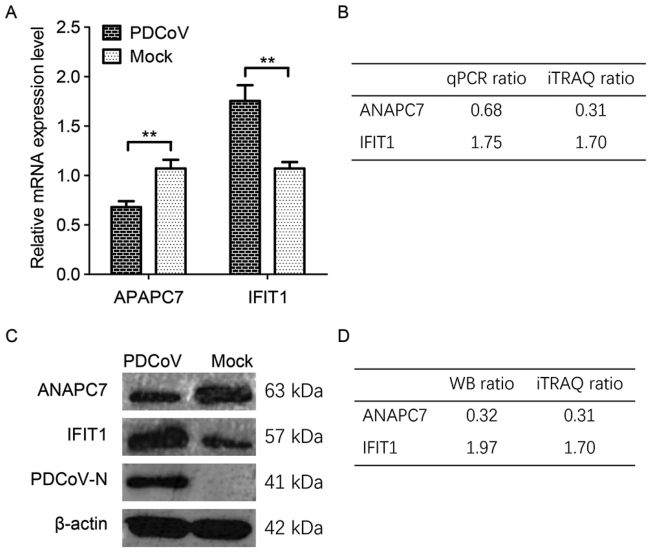

	qPCR ratio	iTRAQ ratio
ANAPC7	0.68	0.31
IFIT1	1.75	1.70

	WB ratio	iTRAQ ratio
ANAPC7	0.32	0.31
IFIT1	1.97	1.70

Figure 2. Validation of the LC-MS/MS results by Western blot analysis. (A) Quantitative real-time PCR (qPCR) analysis of the relative mRNA expression level of ANAPC7 and IFIT1 in IPEC-J2 cells upon PDCoV infection. IPEC-J2 cells were mock infected or infected with the PDCoV CHN-HN-1601 strain at an MOI of 0.1 $TCID_{50}$/cell and collected at 24 hpi. Total RNA was extracted and reverse-transcribed into cDNA for the subsequent analysis via qPCR. Fold-change values were calculated based on the $2^{-\Delta\Delta Ct}$ method, using β-actin as the housekeeping gene. Error bars indicate the standard error of three independent experiments (Student's t test; $^*p < 0.05$). (B) The relative ratio of ANAPC7 and IFIT1 mRNAs normalized to β-actin between PDCoV- and mock-infected cells was calculated based on the qPCR data. The iTRAQ ratio (PDCoV/Mock) obtained by MS analysis was simultaneously shown as a comparison. (C) Western blot (WB) analysis of the expression of ANAPC7 and IFIT1 proteins in IPEC-J2 cells upon PDCoV infection. IPEC-J2 cells were mock infected or infected with the PDCoV CHN-HN-1601 strain at an MOI of 0.1 $TCID_{50}$/cell. At 24 hpi, the cells were harvested and processed for WB analysis using rabbit anti-ANAPC7, mouse anti-IFIT1 polyclonal antibodies and the mAb 1A3 specific for PDCoV. β-Actin was included as an internal loading control. The images shown are representatives of three independent experiments. (D) The optical intensity ratio between the corresponding bands (PDCoV-infected band/Mock band) was measured by densitometric scanning and normalized to the intensity of the β-actin bands in each experiment. The iTRAQ ratio (PDCoV/Mock) obtained by MS analysis was simultaneously shown as a comparison.

multicellular organismal process, developmental process, localization, and so on (Figure 3A; Supplementary File S3), among which those associated with multiorganism process, detoxification, and localization were significantly enriched (Figure 3B); within the CC category, the proteins were predicted to be primarily distributed within 9 different cellular components, such as synapse, extracellular region, membrane, organelle, and cell part (Figure 3A), with the significantly enriched being located in the membrane, organelle and cell part (Figure 3B); and within the MF category, the proteins were predicted to be linked with 8 molecular functions, for instance, structural molecule activity, transporter activity, and antioxidant activity (Figure 3A), but no GO term was identified as significantly enriched within this category (Figure 3B).

3.6. COG Function Classification of the DEPs

To further characterize the DEPs, COG function classification was also applied to categorize the proteins. As shown in Figure 4, the DEPs could be further classified into 18 categories (Supplementary File S4). Among them, 9 proteins were related to general function prediction only; 8 proteins were involved in transcription; 6 proteins were relevant to signal transduction mechanisms; 5 proteins were associated with protein turnover, posttranslational modification, and chaperones; 4 proteins were linked to vesicular transport, intracellular trafficking, and secretion; 4 proteins were correlated with RNA processing and modification; 3 proteins were correlated with chromatin structure and dynamics; 3 proteins were associated with carbohydrate transport and metabolism. Seven proteins were respectively related to one of the following biological functions: nucleotide transport and metabolism; lipid transport and metabolism; translation, ribosomal structure, and biogenesis; cell wall/membrane/envelope biogenesis; inorganic ion transport and metabolism; extracellular structures; and cytoskeleton. Notably, another 7 proteins related to unknown function were also identified (Figure 4). Therefore, further investigation concentrating on the function of these cellular proteins is certainly worth trying in the future.

3.7. KEGG Pathway Analysis of the DEPs

To explore the underlying signaling pathways existing among the identified DEPs, KEGG pathway analyses were done to draw pathway maps.[35] As shown in Figure 5A, the 78 identified DEPs were involved in 26 pathways, among which the top 5 involving more than three proteins were related to viral infectious diseases, signal transduction, immune system, digestive system and cancers. All the DEPs could be further classified into 6 KEGG pathway categories, including organismal systems, metabolism, human diseases, genetic information processing, environmental information processing, and cellular processes (Supplementary File S5). For the upregulated proteins, the top 20 relevant pathways were illustrated in Figure 5B and Supplementary File S6. The signaling pathways of interest included the RIG-I-like receptor signaling pathway, PI3K-AKT signaling pathway, endocytosis, pathways in cancer, etc. For the downregulated proteins, the top 20 relevant pathways were displayed in Figure 5C and Supplementary File S7. The signaling pathways of interest included the mTOR, MAPK, FoxO signaling pathways and so on. Interestingly, one upregulated protein (Secretagogin) and one downregulated protein (AKT2) were simultaneously involved in Fc gamma R-mediated phagocytosis. To further explore the possible involvement of the identified DEPs in the underlying signaling pathways, KEGG pathway enrichment analysis was performed. Our data demonstrated that the DEPs were primarily involved in the HIF-1 signaling pathway, HTLV-I infection, human papillomavirus infection, AGE-RAGE signaling pathway in diabetic complications, central carbon metabolism in cancer, influenza A, measles, Fc gamma R-mediated phagocytosis, small cell lung cancer, glycosaminoglycan biosynthesis, progesterone-mediated oocyte maturation, and relaxin signaling pathway (Figure 5D). These signaling pathways were mainly distributed in four distinct functional categories: environmental information processing, human diseases, metabolism, and organismal systems (Figure 5D).

3.8. Protein−Protein Interaction Networks of the DEPs

To explore the potential protein network connections between the identified DEPs, the web-tool STRING was applied to

https://dx.doi.org/10.1021/acs.jproteome.0c00592
J. Proteome Res. 2020, 19, 4470−4485

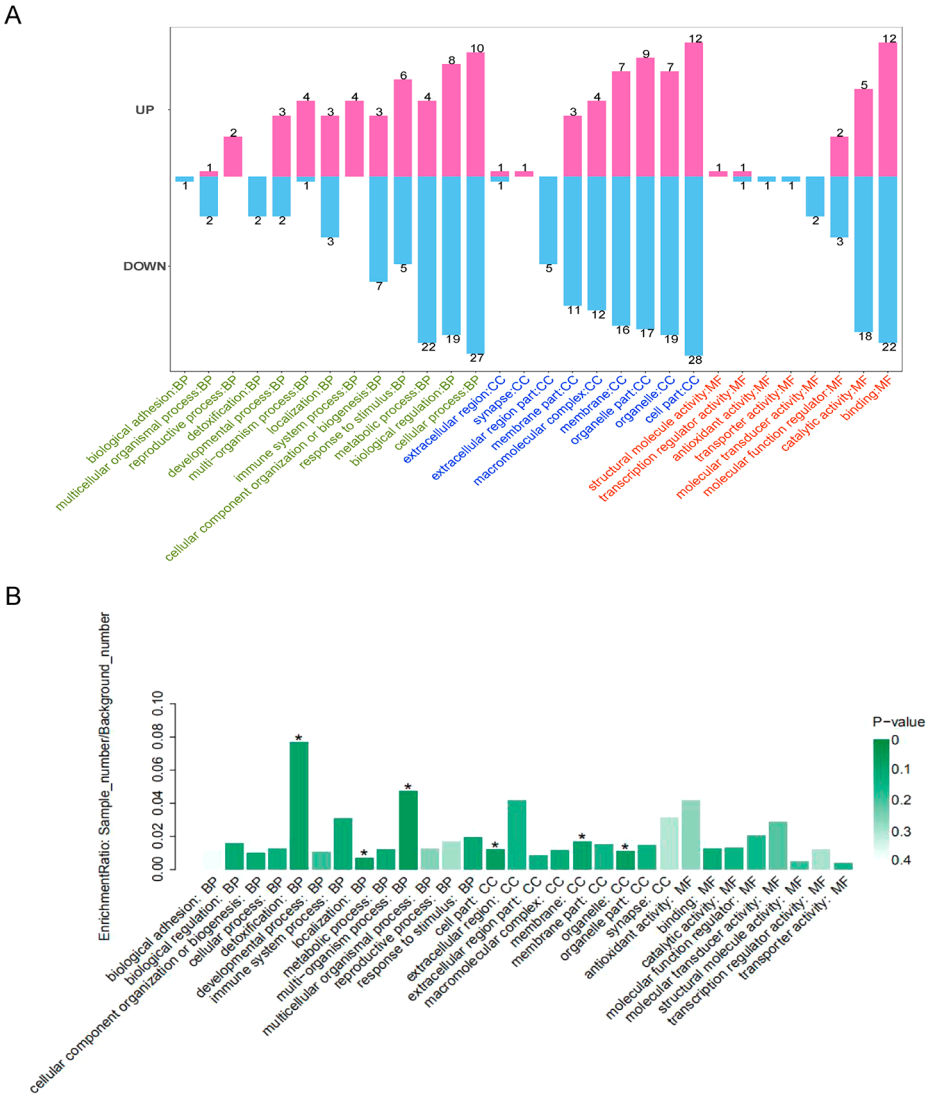

Figure 3. GO functional annotation of the 78 differentially expressed proteins identified in IPEC-J2 cells upon PDCoV infection. (A) GO annotations for the upregulated and downregulated proteins. The proteins were annotated into three major categories: biological process (BP), cellular component (CC), and molecular function (MF). The abscissa text indicates the name and classification of GO terms. The pink and blue columns represent the upregulated and downregulated proteins, respectively, with the number of altered proteins being marked on top of each column. (B) GO enrichment analysis for the upregulated and downregulated proteins. The name and classification of each GO term are indicated in the abscissa. Each column denotes a GO term, and the height of the column represents the enrichment rate. The color implies the significance of the enrichment (p-value), and the darker the color, the more significant the enrichment of the GO term (Fisher's exact test; *$p < 0.05$).

depict protein−protein interaction networks. As shown in Figure 6, the DEPs were mapped to three major functional interaction networks, among which two were tightly connected by a hub protein, ENSSSCG00000000860 (namely NUP37), while the third exists independently. For the two tightly connected networks, they were comprised of two groups of strongly interacted proteins, including SCGN-ISG15-OAS1-IFIT1-IFIT3-ANAPC7-NME7, which are associated with innate immunity, and POLDIP3-NUP37-ERCC6L-DDX55-SMARCA2-NFRB-BAZ2A-HLTF-CHAF1A-CDK9-MNAT1-CTDP1-INTS4, which are associated with cell cycle and cellular components. Of note, at least five proteins act as hub proteins in these two networks tightly connected, including IFIT1, IFIT3, NUP37, SMARCA2, and CDK9. Interestingly, MNAT1 interacted highly with CTDP1 and CDK9, and INTS4 was also well connected to CDK9 (Figure 6). For the third network, there were five proteins with strong interaction in response to PDCoV infection, including MEF2D, VLDLR, LOC780439, PDK1, and AKT2, which are related to cell death and survival. Taken together, these findings further indicate that various functional types of host proteins, various biological functions, and complicated protein networks were affected during PDCoV infection of IPEC-J2 cells, which should provide valuable clues for a better understanding of PDCoV pathogenesis.

4. DISCUSSION

The interactions between host cells and viruses are highly complex, which usually involves numerous alterations in the expression of diverse genes, mRNAs, and proteins.[36,37] Deciphering the laws behind these changes over the course of viral infection plays a vital role in elucidating the pathogenic mechanisms and in developing efficacious antiviral strategies.[37] Over the past decade, MS-based proteomic techniques have

https://dx.doi.org/10.1021/acs.jproteome.0c00592
J. Proteome Res. 2020, 19, 4470−4485

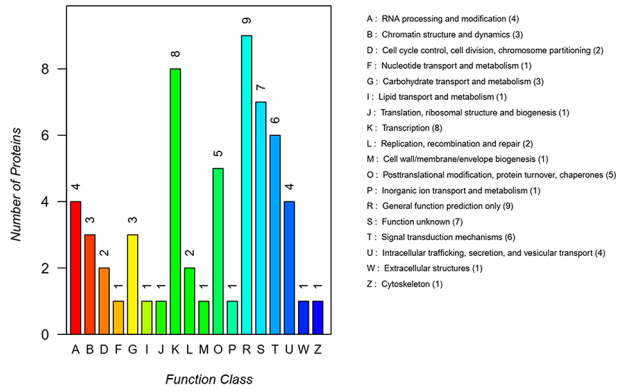

Figure 4. COG function classification of the 78 differentially expressed proteins identified in IPEC-J2 cells upon PDCoV infection. The capital letters in abscissa denote the COG categories as marked on the right of the histogram and the ordinate indicates the number of proteins in each category.

contributed significantly to uncovering more factors and mechanisms related to viral infections and the corresponding host cellular pathophysiological processes.[18] However, no research to date has focused on differential proteomic analysis of global protein profiles in host cells upon infection by PDCoV. In this study, iTRAQ combined with LC-MS/MS was used to identify the DEPs in PDCoV-infected IPEC-J2 cells. Although various cell lines including ST, LLC-PK1, PK-15, and IPI-2I cells have been shown to be highly permissive to PDCoV infection,[17,34,38] considering porcine enterocytes are the natural targets for PDCoV infection in vivo,[8,9] we chose to use IPEC-J2 cells for the proteomic analysis with the goal of obtaining experimental data that could better reflect the physiological state of pigs and the true state of PDCoV infection in vivo. Ultimately, a total of 78 DEPs were identified in PDCoV-infected IPEC-J2 cells, among which 23 proteins were significantly upregulated and 55 proteins were significantly downregulated. Moreover, we also identified six viral proteins including the spike, membrane, nucleocapsid, NS6, NS7, and Nsp5 proteins.

To ensure the reliability of the DEPs identified in the present study, we used qPCR and Western blot to validate two randomly selected DEPs, ANAPC7 and IFIT1, at the transcription and protein expression levels, respectively. In brief, ANAPC7 is an important constituent of the anaphase promoting complex/cyclosome, which is an E3 ubiquitin ligase that regulates the temporal progression of eukaryotic cells by mediating ubiquitination and subsequent 26S proteasome-mediated degradation of key cell cycle regulators.[39] The downregulation of ANAPC7 is indicative of dysfunction of IPEC-J2 cells caused by PDCoV infection. IFIT1 is an innate immune effector molecule that can directly recognize viral single-stranded RNAs carrying a 5′-triphosphate group, thereby inhibiting the expression of viral mRNA.[40] The upregulation of IFIT1 reveals that innate immune responses were activated in PDCoV-infected IPEC-J2 cells to combat with the invading virus. Through the validation of these two DEPs, we found that the obtained proteomics data were reliable and valid, and thus suitable for the subsequent bioinformatics analysis.

First, we made an attempt to assign possible functions to the 78 identified DEPs using GO functional annotation. This tool is an internationally standardized system for gene function classification, which provides a dynamic, updated, controlled vocabularies or ontologies and can well interpret the

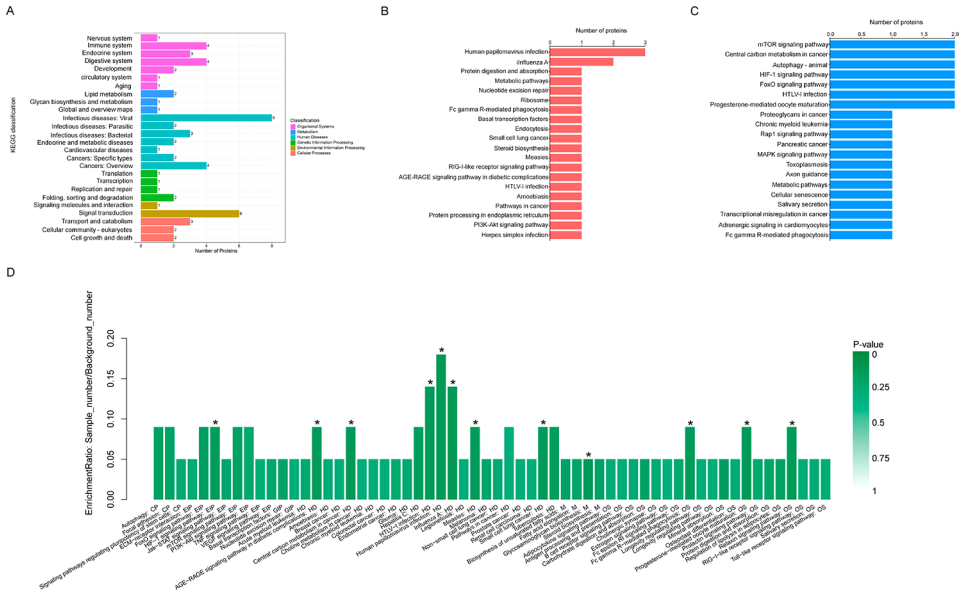

Figure 5. KEGG pathway analysis of the 78 differentially expressed proteins identified in IPEC-J2 cells upon PDCoV infection. (A) KEGG pathway classification of the 78 differentially expressed proteins. The ordinate text indicates the name of biological functions which were classified into 6 KEGG pathway categories, including organismal systems (OS), metabolism (M), human diseases (HD), genetic information processing (GIP), environmental information processing (EIP), and cellular processes (CP). The abscissa displays the number of proteins in each category. (B) The top 20 significant pathways of the significantly upregulated proteins. (C) The top 20 significant pathways of the significantly downregulated proteins. (D) KEGG pathway enrichment analysis of the differentially expressed proteins. The abscissa text displays the name and classification of the KEGG pathways. Each column represents a pathway, and the height of the column implies the enrichment rate. The color manifests the significance of the enrichment (p-value), and the darker the color, the more significant the enrichment of the pathway (Fisher's exact test; $*p < 0.05$).

https://dx.doi.org/10.1021/acs.jproteome.0c00592
J. Proteome Res. 2020, 19, 4470−4485

Figure 6. Protein−protein interaction networks of the 78 differentially expressed proteins identified in IPEC-J2 cells upon PDCoV infection. The networks were built using the STRING database with a minimum interaction score of 0.4 at medium confidence. Each node denotes a protein in the graph; each line is indicative of the interaction between two proteins, and the thicker the line, the closer the mutual relationship. The width of the edges represents the predicted strength of functional associations.

characteristics of target genes and gene products in various organisms.[41] The proteins of our interest involving in different biological functions are listed as follows. Five type I interferon (IFN)-inducible proteins, ISG15, OAS1, Mx1, IFIT1, and IFIT3, were clustered into the BP category associated with the immune system process. Another five cell cycle-regulating proteins, ERCC6L, NME7, NFYB, FOSL1, and CTDP1, were also classified into the BP category but associated with the reproductive process. The nucleolar remodeling complex-constituting protein BAZ2A and the calcium ion binding protein secretagogin were clustered into the same CC category related to synapse.[42,43] The apolipoprotein binding protein VLDLR and the cell cycle control and progression-related protein CDK9 were also divided into the CC category but associated with the macromolecular complex. In addition, three proteins, FOSL1, NUP37, and DDX55, were annotated to be associated with structural molecule activity, transporter activity and catalytic activity, respectively, within the MF category. For further functional annotation of the DEPs, we took a step further by performing COG function classification, which is a widely used tool for analyzing the function and evolution of proteins at the genome scale.[44,45] We discovered that most of the DEPs were assigned new biological functions. For example, the immune system process-related proteins ISG15, OAS1, IFIT1, and IFIT3 categorized by GO functional annotation, were assigned to be involved in signal transduction mechanisms within the COG function classification; the proteins DDX55, SMARCA2, and ERCC6L belonging to three different GO categories were categorized into the same COG category—chromatin structure and dynamics; and the proteins NFYB, FOSL1, and CTDP1 belonging to the same GO category were still in the same COG category—transcription. The aforementioned findings suggested that there exist slight discrepancies in the classification of some proteins between the GO and COG functional annotations. This phenomenon is not unanticipated because the two functional annotation tools are based on different classification criteria.[41,44]

Next, we made an effort to identify the potential signaling pathways that might exist among the DEPs using KEGG pathway analysis, an extensively used method for the integration and interpretation of high-throughput proteomic

https://dx.doi.org/10.1021/acs.jproteome.0c00592
J. Proteome Res. 2020, 19, 4470−4485

and genomic data.[35,46,47] We found that the DEPs were related to multitudinous signaling pathways. The top five pathways containing ≥4 DEPs included the viral infectious disease pathway, which is involved in eight proteins AKT2, IFIT1, RSAD2, NFYB, ANAPC7, COL4A1, Mx1, and ISG15; the signal transduction pathway, which is involved in six proteins AKT2, BNIP3, PDK1, WDR24, TMEM55B, and COL4A1; the immune system pathway, which is involved in four proteins ISG15, IFIT1, OAS1 and IFIT3; the digestive system pathway, which is involved in four proteins AKT2, MT-2A, COL4A1, and cystatin C; and the cancer pathway, which is involved in four proteins PDK1, AKT2, COL4A1, and CDK9. Once again, we found that the same protein can participate in different signaling pathways. For instance, ISG15, a IFN-α-inducible protein that is paramount to the host antiviral innate immunity,[48] was simultaneously involved in two signaling pathways—viral infectious diseases and immune system. IFIT1 (also named p56/ISG56), an innate nucleic acid immune-sensing receptor that can recognize single-stranded viral RNA lacking 2′-*O*-methylation at the 5′-terminus and thus confers antiviral defense function by disrupting the machinery of host translation initiation,[49,50] was also simultaneously related to viral infectious diseases and immune system signaling pathways. By contrast, COL4A1, also known as type IV collagen alpha 1 chain, was simultaneously involved in four of the top five signaling pathways, including viral infectious disease, signal transduction, digestive system, and cancers. This protein is an integral component of basement membranes, which can inhibit the migration, proliferation and tube formation by endothelial cells via binding to α-1/β-1 integrin, and thus becomes a potential therapeutic candidate for targeting tumor angiogenesis.[51,52]

Other interesting signaling pathways included RIG-I-like receptor, PI3K-AKT, mTOR, and autophagy signaling pathways. As an important family of cytosolic pattern recognition receptors, RIG-I is responsible for sensing of the invading viral RNA by recognizing its pathogen-associated molecular patterns to activate downstream signaling cascades, and thereby produce type I IFN.[53,54] The generated IFN molecules then bind to IFN receptors and activate numerous ISGs, which exert critical antiviral innate immune functions either directly or indirectly.[55] In our study, five upregulated proteins encoded by ISGs, including ISG15, OAS1, Mx1, IFIT1, and IFIT3, were identified in PDCoV-infected IPEC-J2 cells. Although these proteins related to type I IFN induction have been reported to participate in diverse viral infections,[22,56] most of them were identified for the first time to be associated with PDCoV infection. These data suggest that the canonical IFN signaling pathways were activated in IPEC-J2 cells upon infection by PDCoV. This was further confirmed by a recent transcriptome-level study which also demonstrated that the RIG-I-like receptor signaling pathway was activated in PDCoV-infected cells, even though a different type of cells, PK-15, was used.[17] Nevertheless, there is increasing evidence suggesting that PDCoV has evolved multiple escape strategies to interfere with the host's innate immunity. For example, the nsp15 of PDCoV was found to be able to antagonize IFN-β production in LLC-PK1 cells by disrupting the phosphorylation and nuclear translocation of nuclear factor-κB p65 subunit, which is independent of its endoribonuclease activity.[57] The Nsp5 of PDCoV was demonstrated to suppress the production of type I IFNs by cleaving the signal transducer and activator of transcription 2, depending on its protease activity.[58] Moreover, the PDCoV accessory protein NS6 was shown to antagonize IFN-β production by disrupting the binding of double-stranded RNA to RIG-I/MDA5 receptors.[59]

Except for the RIG-I-like signaling pathway, two multifunctional signaling pathways, PI3K-AKT and mTOR, were also activated in PDCoV-infected IPEC-J2 cells, both of which participate in regulating autophagy.[60] The PI3K-AKT signaling pathway could be triggered by numerous factors and regulates a variety of fundamental cellular functions, for instance, proliferation and survival.[61] Activated AKT subsequently modulates numerous cellular processes, including cellular autophagy, cell cycle progression and cellular survival.[62] The mTOR signaling pathway is involved in regulating diverse basic biological processes, including lipid biogenesis, protein synthesis, regulation of autophagy, cytoskeletal organization and so on,[63,64] whose dysfunction has been associated with the pathophysiology of many diseases like diabetes and cancer.[65] Although the mTOR and PI3K-AKT signaling pathways are able to negatively and positively regulate autophagy, respectively, in an independent manner,[60,66−68] they usually coregulate autophagy via merging into a single PI3K-AKT-mTOR signaling pathway, which serves as one of the classical pathways for negatively regulating autophagy.[69,70] From the KEGG analysis, we noticed that the PI3K-AKT and mTOR signaling pathways were respectively upregulated and downregulated in PDCoV-infected IPEC-J2 cells, which are the two important indicators of autophagic activation through the PI3K-AKT-mTOR signaling pathway. Accordingly, we speculate that PDCoV infection successfully activated autophagy in IPEC-J2 cells. Our speculation was in agreement with a recent research which revealed that PDCoV infection triggered autophagy in LLC-PK1 cells,[71] despite using a different cell line. Undoubtedly, further studies are definitely needed to confirm the autophagy induced by PDCoV infection, to analyze the impact of autophagy on viral replication and to explore the underlying molecular mechanisms of PDCoV-induced autophagy. It should be noted that the PI3K-AKT-mTOR signaling pathway also plays an important role in many physiological and pathological conditions,[69] except for regulating autophagy.

Finally, we sought to uncover the hidden interaction networks among the DEPs using STRING analysis, and discovered three major functional networks consisting of the RIG-I-like receptor, PDK1-AKT2 and cell cycle signaling pathways. These findings are in accordance with the results of KEGG pathway analysis, thus further consolidating the credibility of these putative signaling pathways involved in PDCoV-infected IPEC-J2 cells. Given the former two signaling pathways have already been discussed earlier, we next focus on the cell cycle signaling pathway. As can be seen from the network diagram (Figure 6), three small networks with NUP37, SMARCA2, and CDK9 as the respective hub proteins together constitute the cell cycle signaling pathway. NUP37 is an important constituent of the nuclear pore Nup107−160 subcomplex, which controls the bidirectional trafficking of macromolecules that traverse the nuclear envelope.[72] SMARCA2 is an important member of the SWI/SNF family with helicase and ATPase activities, and has been shown to regulate numerous biological processes such as cell proliferation and DNA repair.[73] CDK9 paired with cyclin T1 forms the positive transcription elongation factor b (p-TEFb) complex and induces transcriptional activation by hyperphosphorylating RNA polymerase II, and thereby regulating numerous vital

https://dx.doi.org/10.1021/acs.jproteome.0c00592
J. Proteome Res. 2020, 19, 4470−4485

cellular functions including proliferation, differentiation, DNA repair and apoptosis.[74,75] However, growing studies suggest that CDK9 is also related to many pathologic processes, such as cancer, cardiovascular diseases and viral replication.[74] Currently, CDK9 has been demonstrated to be involved in the replication of multiple viruses, such as influenza A virus, dengue virus, human adenovirus, and human immunodeficiency virus.[75] For example, CDK9 was found to interact with the viral RNA-dependent RNA polymerases of influenza A virus and facilitate its association with cellular RNA polymerase II, thereby promoting viral transcription.[76] CDK9 was also shown to be critical for the transcription of viral early genes and the replication of human adenovirus. Treatment of host cells with the CDK9 inhibitor, FIT-039, which functions by suppressing mRNA transcription, can efficiently inhibits the replication of human adenovirus.[77] In the present study, CDK9 was significantly downregulated in IPEC-J2 cells upon PDCoV infection; however, the biological functions hidden behind this change warrant further investigation.

Of note, it is of great significance to compare our proteomics data with those of the newly emergent severe acute respiratory syndrome coronavirus-2 (SARS-CoV-2),[78,79] which caused the Coronavirus Disease 2019 (COVID-19) Pandemic and has posed a serious global public health emergency. Recently, Appelberg et al. conducted an integrative proteo-transcriptomics analysis of Huh7 cells responding to SARS-CoV-2 infection, and identified ErbB, HIF-1, mTOR, and TNF signaling pathways that were significantly regulated during SARS-CoV-2 infection in vitro.[78] They further demonstrated that the Akt inhibitor MK-2206, targeting the mTOR signaling pathway, was able to significantly reduce the replication of SARS-CoV-2. Moreover, another recent study investigated the translatome and proteome of Caco-2 cells in response to SARS-CoV-2 infection in vitro, and discovered that several cellular pathways linked to translation, proteostasis, splicing, carbon metabolism, and nucleotide metabolism were reshaped during viral infection.[79] On this basis, the authors tested two translation inhibitors, cycloheximide and emetine, for their ability to suppress SARS-CoV-2 replication, and found that both pharmaceuticals significantly decreased the replication of SARS-CoV-2 in Caco-2 cells. Undoubtedly, by comparing the similarities and differences of cellular proteomes between PDCoV- and SARS-CoV-2-infected host cells, it is possible to find some common signaling pathways and key adaptor molecules that function to inhibit viral replication, and thus provide valuable clues for screening of therapeutic drugs for PDCoV and designing novel antiviral strategies.

5. CONCLUSIONS

The present study provides the first systematic analysis of the global protein profiles of PDCoV-infected IPEC-J2 cells using a quantitative proteomics approach in which iTRAQ was coupled to LC-MS/MS. A total of 78 DEPs, including 23 upregulated proteins and 55 downregulated proteins, were identified in PDCoV-infected IPEC-J2 cells at 24 hpi. Bioinformatics analyses further revealed that a majority of the DEPs were involved in various crucial biological processes and signaling pathways, such as digestive system, immune system, signal transduction, and RIG-I-like receptor, mTOR, PI3K-AKT, autophagy, and cell cycle signaling pathways. Although further investigations are required to elucidate the functions of the DEPs of interest, our current data provide valuable clues for the in-depth investigation of pathogenic mechanisms of PDCoV and defense mechanisms of host cells.

■ ASSOCIATED CONTENT

Supporting Information

The Supporting Information is available free of charge at https://pubs.acs.org/doi/10.1021/acs.jproteome.0c00592.

Supplementary Figure S1: Repeatability analysis of different biological replicates used for iTRAQ-coupled LC−MS/MS proteomic analysis; Supplementary Figure S2: The original images of the entire PVDF membranes containing the target Western blots of Figure 2C (PDF)

Supplementary File S1: A total of 5502 proteins identified in PDCoV- and mock-infected IPEC-J2 cells using iTRAQ-coupled LC-MS method (XLSX)

Supplementary File S2: Viral proteins identified in PDCoV-infected IPEC-J2 cells (XLSX)

Supplementary File S3: GO function annotation of the 78 differentially expressed proteins (XLSX)

Supplementary File S4: COG function classification of the 78 differentially expressed proteins (XLSX)

Supplementary File S5: KEGG pathway analysis of the 78 differentially expressed proteins (XLSX)

Supplementary File S6: The top 20 KEGG pathway of the 23 significantly upregulated proteins (XLSX)

Supplementary File S7: The top 20 KEGG pathway of the 55 significantly downregulated proteins (XLSX)

■ AUTHOR INFORMATION

Corresponding Authors

Yongning Zhang − *Key Laboratory of Animal Epidemiology of Ministry of Agriculture and Rural Affairs, College of Veterinary Medicine, China Agricultural University, Beijing 100193, PR China*; orcid.org/0000-0002-0134-2761; Email: zhangyongning@cau.edu.cn

Hanchun Yang − *Key Laboratory of Animal Epidemiology of Ministry of Agriculture and Rural Affairs, College of Veterinary Medicine, China Agricultural University, Beijing 100193, PR China*; Email: yanghanchun1@cau.edu.cn

Authors

Xinrong Zhou − *Key Laboratory of Animal Epidemiology of Ministry of Agriculture and Rural Affairs, College of Veterinary Medicine, China Agricultural University, Beijing 100193, PR China*

Lei Zhou − *Key Laboratory of Animal Epidemiology of Ministry of Agriculture and Rural Affairs, College of Veterinary Medicine, China Agricultural University, Beijing 100193, PR China*

Xinna Ge − *Key Laboratory of Animal Epidemiology of Ministry of Agriculture and Rural Affairs, College of Veterinary Medicine, China Agricultural University, Beijing 100193, PR China*

Xin Guo − *Key Laboratory of Animal Epidemiology of Ministry of Agriculture and Rural Affairs, College of Veterinary Medicine, China Agricultural University, Beijing 100193, PR China*

Jun Han − *Key Laboratory of Animal Epidemiology of Ministry of Agriculture and Rural Affairs, College of Veterinary Medicine, China Agricultural University, Beijing 100193, PR China*

Complete contact information is available at: https://pubs.acs.org/10.1021/acs.jproteome.0c00592

https://dx.doi.org/10.1021/acs.jproteome.0c00592
J. Proteome Res. 2020, 19, 4470−4485

Author Contributions

Xinrong Zhou performed the experiments; Lei Zhou, Xinna Ge, Xin Guo, Jun Han, and Yongning Zhang analyzed the experimental data; Xinrong Zhou and Yongning Zhang wrote the paper; and Hanchun Yang designed the experiments and edited the paper.

Notes

The authors declare no competing financial interest.

The proteomics data obtained by LC-MS/MS in this study were deposited to the ProteomeXchange Consortium (http://proteomecentral.proteomexchange.org) by means of the Proteomics Identifications (PRIDE) partner repository with the data set identifier PXD019975.

■ ACKNOWLEDGMENTS

This work was funded by the National Key Research and Development Program (2018YFD0500103; http://program.most.gov.cn/) of the Ministry of Science and Technology of the People's Republic of China, and the China Agriculture Research System (CARS-35) from the Ministry of Agriculture and Rural Affairs of the People's Republic of China.

■ REFERENCES

(1) Jung, K.; Hu, H.; Saif, L. J. Porcine deltacoronavirus infection: etiology, cell culture for virus isolation and propagation, molecular epidemiology and pathogenesis. *Virus Res.* **2016**, *226*, 50−59.

(2) Woo, P. C.; Lau, S. K.; Lam, C. S.; Lau, C. C.; Tsang, A. K.; Lau, J. H.; Bai, R.; Teng, J. L.; Tsang, C. C.; Wang, M.; Zheng, B. J.; Chan, K. H.; Yuen, K. Y. Discovery of seven novel mammalian and avian coronaviruses in the genus deltacoronavirus supports bat coronaviruses as the gene source of alphacoronavirus and betacoronavirus and avian coronaviruses as the gene source of gammacoronavirus and deltacoronavirus. *J. Virol.* **2012**, *86*, 3995−4008.

(3) Wang, L.; Byrum, B.; Zhang, Y. Detection and genetic characterization of deltacoronavirus in pigs, Ohio, USA, 2014. *Emerging Infect. Dis.* **2014**, *20*, 1227−1230.

(4) Zhang, Y.; Cheng, Y.; Xing, G.; Yu, J.; Liao, A.; Du, L.; Lei, J.; Lian, X.; Zhou, J.; Gu, J. Detection and spike gene characterization in porcine deltacoronavirus in China during 2016−2018. *Infect., Genet. Evol.* **2019**, *73*, 151−158.

(5) Pérez-Rivera, C.; Ramírez-Mendoza, H.; Mendoza-Elvira, S.; Segura-Velázquez, R.; Sánchez-Betancourt, J. I. First report and phylogenetic analysis of porcine deltacoronavirus in Mexico. *Transboundary Emerging Dis.* **2019**, *66*, 1436−1441.

(6) Chen, Q.; Gauger, P.; Stafne, M.; Thomas, J.; Arruda, P.; Burrough, E.; Madson, D.; Brodie, J.; Magstadt, D.; Derscheid, R.; Welch, M.; Zhang, J. Pathogenicity and pathogenesis of a United States porcine deltacoronavirus cell culture isolate in 5-day-old neonatal piglets. *Virology* **2015**, *482*, 51−59.

(7) Zhang, J. Porcine deltacoronavirus: overview of infection dynamics, diagnostic methods, prevalence and genetic evolution. *Virus Res.* **2016**, *226*, 71−84.

(8) Jung, K.; Miyazaki, A.; Hu, H.; Saif, L. J. Susceptibility of porcine IPEC-J2 intestinal epithelial cells to infection with porcine deltacoronavirus (PDCoV) and serum cytokine responses of gnotobiotic pigs to acute infection with IPEC-J2 cell culture-passaged PDCoV. *Vet. Microbiol.* **2018**, *221*, 49−58.

(9) Hu, H.; Jung, K.; Vlasova, A. N.; Saif, L. J. Experimental infection of gnotobiotic pigs with the cell-culture-adapted porcine deltacoronavirus strain OH-FD22. *Arch. Virol.* **2016**, *161*, 3421−3434.

(10) Berschneider, H. M. Development of normal cultured small intestinal epithelial cell lines which transport Na and Cl. *Gastroenterology* **1989**, *96*, A41.

(11) Schierack, P.; Nordhoff, M.; Pollmann, M.; Weyrauch, K. D.; Amasheh, S.; Lodemann, U.; Jöres, J.; Tachu, B.; Kleta, S.; Blikslager, A.; Tedin, K.; Wieler, L. H. Characterization of a porcine intestinal epithelial cell line for in vitro studies of microbial pathogenesis in swine. *Histochem. Cell Biol.* **2006**, *125*, 293−305.

(12) Liu, F.; Li, G.; Wen, K.; Bui, T.; Cao, D.; Zhang, Y.; Yuan, L. Porcine small intestinal epithelial cell line (IPEC-J2) of rotavirus infection as a new model for the study of innate immune responses to rotaviruses and probiotics. *Viral Immunol.* **2010**, *23*, 135−49.

(13) Chen, J.; Wang, H.; Jin, L.; Wang, L.; Huang, X.; Chen, W.; Yan, M.; Liu, G. Profile analysis of circRNAs induced by porcine endemic diarrhea virus infection in porcine intestinal epithelial cells. *Virology* **2019**, *527*, 169−179.

(14) Ma, X.; Zhao, X.; Zhang, Z.; Guo, J.; Guan, L.; Li, J.; Mi, M.; Huang, Y.; Tong, D. Differentially expressed non-coding RNAs induced by transmissible gastroenteritis virus potentially regulate inflammation and NF-κB pathway in porcine intestinal epithelial cell line. *BMC Genomics* **2018**, *19*, 747.

(15) Zhang, H.; Guo, X.; Ge, X.; Chen, Y.; Sun, Q.; Yang, H. Changes in the cellular proteins of pulmonary alveolar macrophage infected with porcine reproductive and respiratory syndrome virus by proteomics analysis. *J. Proteome Res.* **2009**, *8*, 3091−3097.

(16) Manzoni, C.; Kia, D. A.; Vandrovcova, J.; Hardy, J.; Wood, N. W.; Lewis, P. A.; Ferrari, R. Genome, transcriptome and proteome: the rise of omics data and their integration in biomedical sciences. *Briefings Bioinf.* **2018**, *19*, 286−302.

(17) Jiang, S.; Li, F.; Li, X.; Wang, L.; Zhang, L.; Lu, C.; Zheng, L.; Yan, M. Transcriptome analysis of PK-15 cells in innate immune response to porcine deltacoronavirus infection. *PLoS One* **2019**, *14*, No. e0223177.

(18) Aslam, B.; Basit, M.; Nisar, M. A.; Khurshid, M.; Rasool, M. H. Proteomics: technologies and their applications. *J. Chromatogr. Sci.* **2017**, *55*, 182−196.

(19) Jiang, X. S.; Tang, L. Y.; Dai, J.; Zhou, H.; Li, S. J.; Xia, Q. C.; Wu, J. R.; Zeng, R. Quantitative analysis of severe acute respiratory syndrome (SARS)-associated coronavirus-infected cells using proteomic approaches: implications for cellular responses to virus infection. *Mol. Cell. Proteomics* **2005**, *4*, 902−913.

(20) Chen, X.; Wei, S.; Ji, Y.; Guo, X.; Yang, F. Quantitative proteomics using SILAC: Principles, applications, and developments. *Proteomics* **2015**, *15*, 3175−3192.

(21) Guan, X.; Rastogi, N.; Parthun, M. R.; Freitas, M. A. Discovery of histone modification crosstalk networks by stable isotope labeling of amino acids in cell culture mass spectrometry (SILAC MS). *Mol. Cell. Proteomics* **2013**, *12*, 2048−2059.

(22) An, K.; Fang, L.; Luo, R.; Wang, D.; Xie, L.; Yang, J.; Chen, H.; Xiao, S. Quantitative proteomic analysis reveals that transmissible gastroenteritis virus activates the JAK-STAT1 signaling pathway. *J. Proteome Res.* **2014**, *13*, 5376−5390.

(23) Moulder, R.; Goo, Y. A.; Goodlett, D. R. Label-free quantitation for clinical proteomics. *Methods Mol. Biol.* **2016**, *1410*, 65−76.

(24) Guo, X.; Hu, H.; Chen, F.; Li, Z.; Ye, S.; Cheng, S.; Zhang, M.; He, Q. iTRAQ-based comparative proteomic analysis of Vero cells infected with virulent and CV777 vaccine strain-like strains of porcine epidemic diarrhea virus. *J. Proteomics* **2016**, *130*, 65−75.

(25) Zhu, Z.; Yang, F.; Zhang, K.; Cao, W.; Jin, Y.; Wang, G.; Mao, R.; Li, D.; Guo, J.; Liu, X.; Zheng, H. Comparative proteomic analysis of wild-type and SAP domain mutant foot-and-mouth disease virus-infected porcine cells identifies the ubiquitin-activating enzyme UBE1 required for virus replication. *J. Proteome Res.* **2015**, *14*, 4194−4206.

(26) Zhou, N.; Fan, C.; Liu, S.; Zhou, J.; Jin, Y.; Zheng, X.; Wang, Q.; Liu, J.; Yang, H.; Gu, J.; Zhou, J. Cellular proteomic analysis of porcine circovirus type 2 and classical swine fever virus coinfection in porcine kidney-15 cells using isobaric tags for relative and absolute quantitation-coupled LC-MS/MS. *Electrophoresis* **2017**, *38*, 1276−1291.

(27) Reed, L. J.; Muench, H. A simple method of estimating fifty percent endpoints. *Am. J. Epidemiol.* **1938**, *27*, 493−497.

(28) Zhang, X. Q.; Bai, L.; Sun, H. B.; Yang, C.; Cai, B. Y. Transcriptomic and proteomic analysis revealed the effect of

https://dx.doi.org/10.1021/acs.jproteome.0c00592
J. Proteome Res. 2020, 19, 4470−4485

funneliformis mosseae in soybean roots differential expression genes and proteins. *J. Proteome Res.* **2020**, *19*, 3631−3643.
(29) Cui, Y. H.; Liu, Q.; Xu, Z. Y.; Li, J. H.; Hu, Z. X.; Li, M. J.; Zheng, W. L.; Li, Z. J.; Pan, H. W. Quantitative proteomic analysis of human corneal epithelial cells infected with HSV-1. *Exp. Eye Res.* **2019**, *185*, 107664.
(30) Yang, S.; Pei, Y.; Zhao, A. iTRAQ-based proteomic analysis of porcine kidney epithelial PK15 cells infected with pseudorabies virus. *Sci. Rep.* **2017**, *7*, 45922.
(31) Xie, C.; Mao, X.; Huang, J.; Ding, Y.; Wu, J.; Dong, S.; Kong, L.; Gao, G.; Li, C. Y.; Wei, L. KOBAS 2.0: a web server for annotation and identification of enriched pathways and diseases. *Nucleic Acids Res.* **2011**, *39*, W316−322.
(32) Szklarczyk, D.; Gable, A. L.; Lyon, D.; Junge, A.; Wyder, S.; Huerta-Cepas, J.; Simonovic, M.; Doncheva, N. T.; Morris, J. H.; Bork, P.; Jensen, L. J.; Mering, C. V. STRING v11: protein-protein association networks with increased coverage, supporting functional discovery in genome-wide experimental datasets. *Nucleic Acids Res.* **2019**, *47*, D607−613.
(33) Livak, K. J.; Schmittgen, T. D. Analysis of relative gene expression data using real-time quantitative PCR and the $2^{-\Delta\Delta Ct}$ method. *Methods* **2001**, *25*, 402−408.
(34) Hu, H.; Jung, K.; Vlasova, A. N.; Chepngeno, J.; Lu, Z.; Wang, Q.; Saif, L. J. Isolation and characterization of porcine deltacoronavirus from pigs with diarrhea in the United States. *J. Clin. Microbiol.* **2015**, *53*, 1537−1548.
(35) Kanehisa, M.; Furumichi, M.; Tanabe, M.; Sato, Y.; Morishima, K. KEGG: new perspectives on genomes, pathways, diseases and drugs. *Nucleic Acids Res.* **2017**, *45*, D353−361.
(36) Brito, A. F.; Pinney, J. W. Protein-protein interactions in virus-host systems. *Front. Microbiol.* **2017**, *8*, 1557.
(37) Ramage, H.; Cherry, S. Virus-host interactions: from unbiased genetic screens to function. *Annu. Rev. Virol.* **2015**, *2*, 497−524.
(38) Zhang, J.; Chen, J.; Shi, D.; Shi, H.; Zhang, X.; Liu, J.; Cao, L.; Zhu, X.; Liu, Y.; Wang, X.; Ji, Z.; Feng, L. Porcine deltacoronavirus enters cells via two pathways: a protease-mediated one at the cell surface and another facilitated by cathepsins in the endosome. *J. Biol. Chem.* **2019**, *294*, 9830−9843.
(39) Turnell, A. S.; Stewart, G. S.; Grand, R. J. A.; Rookes, S. M.; Martin, A.; Yamano, H.; Elledge, S. J.; Gallimore, P. H. The APC/C and CBP/p300 cooperate to regulate transcription and cell-cycle progression. *Nature* **2005**, *438*, 690−695.
(40) Habjan, M.; Hubel, P.; Lacerda, L.; Benda, C.; Holze, C.; Eberl, C. H.; Mann, A.; Kindler, E.; Gil-Cruz, C.; Ziebuhr, J.; Thiel, V.; Pichlmair, A. Sequestration by IFIT1 impairs translation of 2′O-unmethylated capped RNA. *PLoS Pathog.* **2013**, *9*, e1003663.
(41) Di Lena, P.; Domeniconi, G.; Margara, L.; Moro, G. GOTA: GO term annotation of biomedical literature. *BMC Bioinf.* **2015**, *16*, 346.
(42) Kosaka, T.; Kosaka, K. Calcium-binding protein, secretagogin, specifies the microcellular tegmental nucleus and intermediate and ventral parts of the cuneiform nucleus of the mouse and rat. *Neurosci. Res.* **2018**, *134*, 30−38.
(43) Gu, L.; Frommel, S. C; Oakes, C. C; Simon, R.; Grupp, K.; Gerig, C. Y; Bar, D.; Robinson, M. D; Baer, C.; Weiss, M.; Gu, Z.; Schapira, M.; Kuner, R.; Sultmann, H.; Provenzano, M.; Yaspo, M.-L.; Brors, B.; Korbel, J.; Schlomm, T.; Sauter, G.; Eils, R.; Plass, C.; Santoro, R. BAZ2A (TIP5) is involved in epigenetic alterations in prostate cancer and its overexpression predicts disease recurrence. *Nat. Genet.* **2015**, *47*, 22−30.
(44) Tatusov, R. L.; Galperin, M. Y.; Natale, D. A.; Koonin, E. V. The COG database: a tool for genome-scale analysis of protein functions and evolution. *Nucleic Acids Res.* **2000**, *28*, 33−36.
(45) Tatusov, R. L.; Fedorova, N. D.; Jackson, J. D.; Jacobs, A. R.; Kiryutin, B.; Koonin, E. V.; Krylov, D. M.; Mazumder, R.; Mekhedov, S. L.; Nikolskaya, A. N.; Rao, B. S.; Smirnov, S.; Sverdlov, A. V.; Vasudevan, S.; Wolf, Y. I.; Yin, J. J.; Natale, D. A. The COG database: an updated version includes eukaryotes. *BMC Bioinf.* **2003**, *4*, 41.
(46) Kanehisa, M.; Sato, Y.; Furumichi, M.; Morishima, K.; Tanabe, M. New approach for understanding genome variations in KEGG. *Nucleic Acids Res.* **2019**, *47*, D590−595.
(47) Kanehisa, M. Toward understanding the origin and evolution of cellular organisms. *Protein Sci.* **2019**, *28*, 1947−1951.
(48) Perng, Y. C.; Lenschow, D. J. ISG15 in antiviral immunity and beyond. *Nat. Rev. Microbiol.* **2018**, *16*, 423−439.
(49) Hartmann, G. Nucleic Acid Immunity. *Adv. Immunol.* **2017**, *133*, 121−169.
(50) Hyde, J. L.; Diamond, M. S. Innate immune restriction and antagonism of viral RNA lacking 2-O methylation. *Virology* **2015**, *479−480*, 66−74.
(51) Volonghi, I.; Pezzini, A.; Del Zotto, E.; Giossi, A.; Costa, P.; Ferrari, D.; Padovani, A. Role of COL4A1 in basement-membrane integrity and cerebral small-vessel disease. The COL4A1 stroke syndrome. *Curr. Med. Chem.* **2010**, *17*, 1317−1324.
(52) Meuwissen, M. E.; Halley, D. J.; Smit, L. S.; Lequin, M. H.; Cobben, J. M.; de Coo, R.; van Harssel, J.; Sallevelt, S.; Woldringh, G.; van der Knaap, M. S.; de Vries, L. S.; Mancini, G. M. The expanding phenotype of COL4A1 and COL4A2 mutations: clinical data on 13 newly identified families and a review of the literature. *Genet. Med.* **2015**, *17*, 843−853.
(53) Wu, B.; Hur, S. How RIG-I like receptors activate MAVS. *Curr. Opin. Virol.* **2015**, *12*, 91−98.
(54) Yoneyama, M.; Onomoto, K.; Jogi, M.; Akaboshi, T.; Fujita, T. Viral RNA detection by RIG-I-like receptors. *Curr. Opin. Immunol.* **2015**, *32*, 48−53.
(55) Schneider, W. M.; Chevillotte, M. D.; Rice, C. M. Interferon-stimulated genes: a complex web of host defenses. *Annu. Rev. Immunol.* **2014**, *32*, 513−545.
(56) Pfaff, F.; Hagglund, S.; Zoli, M.; Blaise-Boisseau, S.; Laloy, E.; Koethe, S.; Zuhlke, D.; Riedel, K.; Zientara, S.; Bakkali-Kassimi, L.; Valarcher, J. F.; Hoper, D.; Beer, M.; Eschbaumer, M. Proteogenomics uncovers critical elements of host response in bovine soft palate epithelial cells following in vitro infection with foot-and-mouth disease virus. *Viruses* **2019**, *11*, 53.
(57) Liu, X.; Fang, P.; Fang, L.; Hong, Y.; Zhu, X.; Wang, D.; Peng, G.; Xiao, S. Porcine deltacoronavirus nsp15 antagonizes interferon-β production independently of its endoribonuclease activity. *Mol. Immunol.* **2019**, *114*, 100−107.
(58) Zhu, X.; Wang, D.; Zhou, J.; Pan, T.; Chen, J.; Yang, Y.; Lv, M.; Ye, X.; Peng, G.; Fang, L.; Xiao, S. Porcine deltacoronavirus Nsp5 antagonizes type I interferon signaling by cleaving STAT2. *J. Virol.* **2017**, *91*, e00003-17.
(59) Fang, P.; Fang, L.; Ren, J.; Hong, Y.; Liu, X.; Zhao, Y.; Wang, D.; Peng, G.; Xiao, S. Porcine deltacoronavirus accessory protein NS6 antagonizes interferon beta production by interfering with the binding of RIG-I/MDA5 to double-stranded RNA. *J. Virol.* **2018**, *92*, e00712-18.
(60) Saxton, R. A.; Sabatini, D. M. mTOR signaling in growth, metabolism, and disease. *Cell* **2017**, *168*, 960−976.
(61) Porta, C.; Figlin, R. A. Phosphatidylinositol-3-kinase/Akt signaling pathway and kidney cancer, and the therapeutic potential of phosphatidylinositol-3-kinase/Akt inhibitors. *J. Urol.* **2009**, *182*, 2569−2577.
(62) Hers, I.; Vincent, E. E.; Tavare, J. M. Akt signalling in health and disease. *Cell. Signalling* **2011**, *23*, 1515−1527.
(63) Luo, Y.; Xu, W.; Li, G.; Cui, W. Weighing in on mTOR complex 2 signaling: the expanding role in cell metabolism. *Oxid. Med. Cell. Longevity* **2018**, *2018*, 7838647.
(64) Yang, Q.; Guan, K. L. Expanding mTOR signaling. *Cell Res.* **2007**, *17*, 666−681.
(65) Abraham, R. T. Regulation of the mTOR signaling pathway: from laboratory bench to bedside and back again. *F1000 Biol. Rep.* **2009**, *1*, 8.
(66) Liu, J.; Liu, L.; Tian, Z.; Li, Y.; Shi, C.; Shi, J.; Wei, S.; Zhao, Y.; Zhang, C.; Bai, B.; Chen, Z.; Zhang, H. In silico discovery of a small molecule suppressing lung carcinoma A549 cells proliferation and

https://dx.doi.org/10.1021/acs.jproteome.0c00592
J. Proteome Res. 2020, 19, 4470−4485

inducing autophagy via mTOR pathway inhibition. *Mol. Pharmaceutics* **2018**, *15*, 5427−5436.
(67) Ravikumar, B.; Vacher, C.; Berger, Z.; Davies, J. E.; Luo, S.; Oroz, L. G.; Scaravilli, F.; Easton, D. F.; Duden, R.; O'Kane, C. J.; Rubinsztein, D. C. Inhibition of mTOR induces autophagy and reduces toxicity of polyglutamine expansions in fly and mouse models of Huntington disease. *Nat. Genet.* **2004**, *36*, 585−595.
(68) Wang, Y.; Zhang, H. Regulation of autophagy by mTOR signaling pathway. *Adv. Exp. Med. Biol.* **2019**, *1206*, 67−83.
(69) Heras-Sandoval, D.; Pérez-Rojas, J. M.; Hernandez-Damián, J.; Pedraza-Chaverri, J. The role of PI3K/AKT/mTOR pathway in the modulation of autophagy and the clearance of protein aggregates in neurodegeneration. *Cell. Signalling* **2014**, *26*, 2694−2701.
(70) Dikic, I.; Elazar, Z. Mechanism and medical implications of mammalian autophagy. *Nat. Rev. Mol. Cell Biol.* **2018**, *19*, 349−364.
(71) Qin, P.; Du, E. Z.; Luo, W. T.; Yang, Y. L.; Zhang, Y. Q.; Wang, B.; Huang, Y. W. Characteristics of the life cycle of porcine deltacoronavirus (PDCoV) in vitro: replication kinetics, cellular ultrastructure and virion morphology, and evidence of inducing autophagy. *Viruses* **2019**, *11*, 455.
(72) Chen, J.; Wo, D.; Ma, E.; Yan, H.; Peng, J.; Zhu, W.; Fang, Y.; Ren, D. N. Deletion of low-density lipoprotein-related receptor 5 inhibits liver cancer cell proliferation via destabilizing nucleoporin 37. *Cell Commun. Signaling* **2019**, *17*, 174.
(73) Zhang, Z.; Wang, F.; Du, C.; Guo, H.; Ma, L.; Liu, X.; Kornmann, M.; Tian, X.; Yang, Y. BRM/SMARCA2 promotes the proliferation and chemoresistance of pancreatic cancer cells by targeting JAK2/STAT3 signaling. *Cancer Lett.* **2017**, *402*, 213−224.
(74) Franco, L. C.; Morales, F.; Boffo, S.; Giordano, A. CDK9: a key player in cancer and other diseases. *J. Cell. Biochem.* **2018**, *119*, 1273−1284.
(75) Zaborowska, J.; Isa, N. F.; Murphy, S. P-TEFb goes viral. *BioEssays* **2016**, *38*, S75−85.
(76) Zhang, J.; Li, G.; Ye, X. Cyclin T1/CDK9 interacts with influenza A virus polymerase and facilitates its association with cellular RNA polymerase II. *J. Virol.* **2010**, *84*, 12619−12627.
(77) Yamamoto, M.; Onogi, H.; Kii, I.; Yoshida, S.; Iida, K.; Sakai, H.; Abe, M.; Tsubota, T.; Ito, N.; Hosoya, T.; Hagiwara, M. CDK9 inhibitor FIT-039 prevents replication of multiple DNA viruses. *J. Clin. Invest.* **2014**, *124*, 3479−3488.
(78) Appelberg, S.; Gupta, S.; Akusjärvi, S. S.; Ambikan, A. T.; Mikaeloff, F.; Saccon, E.; Végvári, Á.; Benfeitas, R.; Sperk, M.; Ståhlberg, M.; Krishnan, S.; Singh, K.; Penninger, J. M.; Mirazimi, A.; Neogi, U. Dysregulation in Akt/mTOR/HIF-1 signaling identified by proteo-transcriptomics of SARS-CoV-2 infected cells. *Emerg. Emerging Microbes Infect.* **2020**, *9*, 1748−1760.
(79) Bojkova, D.; Klann, K.; Koch, B.; Widera, M.; Krause, D.; Ciesek, S.; Cinatl, J.; Münch, C. Proteomics of SARS-CoV-2-infected host cells reveals therapy targets. *Nature* **2020**, *583*, 469−472.

https://dx.doi.org/10.1021/acs.jproteome.0c00592
J. Proteome Res. 2020, 19, 4470−4485